

RL-RC-DoT: A Block-level RL agent for Task-Aware Video Compression

Uri Gadot
NVIDIA Research

uri.gad@campus.technion.ac.il

Assaf Shocher
NVIDIA Research

ashocher@nvidia.com

Shie Mannor
NVIDIA Research

smannor@nvidia.com

Gal Chechik
NVIDIA Research
gchechik@nvidia.com

Assaf Hallak
NVIDIA Research
ahallak@nvidia.com

January 22, 2025

Abstract

Video encoders optimize compression for human perception by minimizing reconstruction error under bit-rate constraints. In many modern applications such as autonomous driving, an overwhelming majority of videos serve as input for AI systems performing tasks like object recognition or segmentation, rather than being watched by humans. It is therefore useful to optimize the encoder for a downstream task instead of for perceptual image quality. However, a major challenge is how to combine such downstream optimization with existing standard video encoders, which are highly efficient and popular. Here, we address this challenge by controlling the Quantization Parameters (QPs) at the macro-block level to optimize the downstream task. This granular control allows us to prioritize encoding for task-relevant regions within each frame. We formulate this optimization problem as a Reinforcement Learning (RL) task, where the agent learns to balance long-term implications of choosing QPs on both task performance and bit-rate constraints. Notably, our policy does not require the downstream task as an input during inference, making it suitable for streaming applications and edge devices such as vehicles. We demonstrate significant improvements in two tasks, car detection, and ROI (saliency) encoding. Our approach improves task performance for a given bit rate compared to traditional task

agnostic encoding methods, paving the way for more efficient task-aware video compression.

1 Introduction

Video compression is an essential and widely studied problem [1, 3, 16, 32, 37]. Most video compression algorithms are designed for preserving how a video is perceived by people. With the success of computer vision applications, many videos are used in automated systems, from autonomous drones and cars, to security cameras, and in downstream tasks, like object detection or recognition. In these cases, compression must prioritize regions relevant to the task at hand (e.g., allocating more bits to objects than to the background).

Real-world deployment of compression and computer vision systems complicates matters further. Video data must be collected in real time from devices, using low computational resources, and be usable for training various models across multiple tasks, not just for immediate inference. Furthermore, due to computational and hardware constraints, compression must be done without access to the ground truth for the downstream tasks during the encoding process. Our goal is to tackle these challenges by providing a general video compression method that can be adapted to any task, any encoding standard, operates in real-time, imposes low computational de-

mands on the encoding side, and requires no ground-truth labels.

Two previous approaches were taken to this problem. The first relies on standardized video encoders [25, 32] which are highly efficient but are not designed for adapting compression to specific tasks in real-time. To address that, previous studies used downstream task information as input to the encoder side [18, 29, 41]. As one example, [41] performs semantic compression by applying a heavy feature extractor before encoding using a ground-truth segmentation maps. This approach may compress well at this setup, but typically require large computation resources before encoding, can not be used for various tasks, and is unsuitable for data collection. A second approach relies on deep encoding [22]. Once again it is computationally expensive and currently unsuitable for real-time applications or resource-constrained environments.

In this paper, we propose RL-RC-DoT, a novel solution to the problem of tuning an efficient real-time video compression system to a downstream task without access to its ground truth labels during inference. Our approach integrates a lightweight network on the video encoder side, trained to control the encoding process such that the decoded output is ideal for the task at hand. By leveraging standardized codecs, we ensure that our method is both computationally efficient and easily deployable across a range of devices. The solution allows for real-time video compression without requiring ground truth for downstream tasks. Our solution can be applied over any existing encoder, for simplicity, we chose to implement it over x264 as a mere example.

Coping with these challenges is hard. Standardized encoders are not differentiable, making it difficult to optimize bit allocation for specific tasks. To overcome this, we introduce a reinforcement learning (RL) mechanism that controls the Quantization Parameter (QP) at the macro-block level, adjusting the bit allocation for each block of the frame dynamically. This allows us to efficiently manage the bit-rate budget while optimizing task performance over an entire sequence of video frames. Our experiments demonstrate that this approach yields significant improvements in rate-distortion trade-offs, not just for the task the encoder was trained on, but also for other related tasks, showcasing the robustness of our method. Furthermore, we demonstrate its generalizability by showing how an encoder trained on one model can

improve performance for other models without additional tuning.

In summary, this paper makes the following contributions. (1) We design the first task-aware video compression method that builds on top of existing encoders and does not require solving the task during inference. (2) We show how to optimize the quantization parameter of every macro-block in the frame while optimizing the performance of a downstream task on the reconstructed video under bit-rate constraints. (3) We design an architecture that outputs multiple actions, a tailored reward for this problem, and a task-prediction loss term. (4) We show improved rate-distortion trade-off for our agent on two tasks, car detection and ROI encoding with only small interference to image quality, and further show robustness to task shift, when tested on a related-but-different task than used for training.

1.1 Related Works

Video compression with RL. The integration of reinforcement learning into video compression has gained significant attention in recent years. Several approaches have focused on frame-level QP optimization [5, 11, 23, 24], using various techniques such as two-pass encoding and dual-critic architectures. While some researchers have proposed more granular control by developing QP selection agents at the Coding Tree Unit (CTU) or MacroBlock (MB) level [12, 13], these methods have been primarily validated only on image compression or intra-mode encoding scenarios.

Task-aware video compression with unrestricted compute. Several previous studies proposed video compression methods that are aware of a downstream task. [44] explored content-specific filters to improve post-processing in video codecs, optimizing them for machine vision tasks like object detection and segmentation. [10] introduced an encoder control for deep video compression that adapts to multiple tasks using a single pre-trained decoder, showing significant bit-rate improvement for object detection and tracking. [30] highlighted the limitations of classical codecs in medical videos, proposing learned compression models to allocate more bits to medically relevant regions. [7] presented a semantic video encoding system that enhances object detection by selectively decompressing frames in surveillance streams. [17] de-

veloped a distributed compression framework that adjusts to varying bandwidth in multi-sensor networks to optimize task performance. [39] introduced an annotation-free optimization strategy that aligns video coding with machine tasks, improving rate savings without relying on ground truth data. Additionally, While [40] focused on real-time, quality-scalable video decoding, it also evaluated the codec performance on machine-based tasks.

All these approaches share a common limitation, they do not use the existing highly optimized and widely prevalent existing video compression ecosystem like the open-source x264 [25]. The challenge therefore remains to design video compression systems that build on top of existing technology, but can be tuned in a-content adaptive way to a set of downstream tasks.

Task-aware video compression with standard encoders Another body of works does employ standardized encoders, but does not consider the inter-frame dependencies. [31] and [8] optimize the CTU partitioning to improve the compression for a downstream task. [9] uses a threshold on the saliency map to allocate more bits to important regions, while [4] optimizes over the modelled relation between each block parameter and the task performance. [18] uses RL for optimizing macro-block QPs, but does so in each frame separately, where the sequence is defined over the sequence of macro-blocks in the same frame. In our work we output all macro-block QPs with one policy and the sequence is defined over consecutive encoded frames in the video. The work most related to ours is [41], where they propose to use RL on both the QPs and macro-block QPs in a hierarchical manner. However, they limit their optimization to only two frames in every GOP, and only two values of macro-block QPs are chosen per block according to a given segmentation map. In our work we optimize over all frames and macro-block QPs, and we do not use any additional information like saliency, segmentation or downstream task during inference.

2 Preliminaries

2.1 Video Compression

Video compression is a process of reducing the size of digital video files while maintaining acceptable visual

quality. It is a crucial technology in the modern digital age, enabling efficient storage, transmission, and streaming of video content across various platforms and devices. The primary goal of video compression is to eliminate redundant and less perceptible information from the video data according to constraints such as bit-rate of the target video.

One key aspect of video compression is the use of Quantization Parameters (QP). QP values control the level of compression and distortion applied to the video data, with higher values resulting in more compression but lower quality, and lower values preserving more detail but producing larger file sizes. In video encoding, QP can be applied at different levels of granularity. Frame QP refers to setting a single QP value for an entire frame, which is useful for maintaining consistent quality across the frame but may not be optimal for all areas. Per-macro-block (MB) QP, conversely, allows for finer control by assigning different QP values to individual MBs within a frame, usually in small perturbations from a pre-assigned frame QP. This approach enables the encoder to apply more compression to less important or visually complex areas while preserving quality in critical regions. Per-MB QP can lead to more efficient compression and better overall visual quality, as it adapts to the local characteristics of the video content. It is especially suitable for task-aware optimization since most tasks target specific areas in the picture (for instance object detection and segmentation).

The effectiveness of video compression is typically measured by comparing the compressed video's file size and visual quality to the original. Metrics like Peak Signal-to-Noise Ratio (PSNR) and Structural Similarity Index Measure (SSIM; [36]) are often used to objectively assess quality. When comparing two encoders the compression efficiency is usually considered. To do so, a video is encoded in several desired bit-rates with each encoder to form a rate-distortion (RD) curve, where the y axis is the quality measure, e.g. PSNR. If one encoder's curve is shifted-left than the other, it means it requires less bits to reach the same quality, rendering it more efficient. If we integrate over the entire curve, and average the result over multiple videos, we obtain a quantity specifying how much bits saves one encoder than the other, a quantity referred to as Bjontegaard delta rate (BD-rate) [38].

With the increasing usages of videos for machine vision, many researchers have recognized the need for task-

aware compression and proposed a suitable evaluation metric [15, 29]. The most straightforward metric which we also use in this paper is obtained by replacing the PSNR in the RD-curve (the y -axis) with a task-specific loss measure such as mIOU or detection precision and calculating the BD-rate with respect to the adjusted curves.

One may wonder, if a downstream task is given, why is video compression needed at all? For instance, in the autonomous vehicle example, if a car detector is available, why not run that detector on the vehicle, and save only its decision instead of the compressed video. There are several strong reasons not to take this approach: (1) Many downstream tasks require resource-heavy networks that cannot run efficiently on-device, making it impractical to process the data locally. (2) Sending only task-specific features limits human interpretability, as there would be no watchable video for explainability. (3) This also confines the data to a single task, preventing its reuse for other applications or analyses. (4) Large-scale data collection, such as in autonomous driving, depends on compressed video storage; using features alone would limit future training and fine-tuning opportunities. (5) Task-specific features are often tied to a particular model, making them incompatible with new models, while compressed video remains adaptable across different systems. We show that our method allows different models to achieve high performance using the same compressed data. This is also the reason why we aim to develop a method that still preserves a video that would be meaningful to a person.

2.2 Reinforcement Learning

Reinforcement Learning (RL; [33]) is a field dealing with sequential decision making in unknown environments. To formulate a problem using RL, we first need to define its underlying Markov Decision Process (MDP). An MDP is defined by a tuple $(\mathcal{S}, \mathcal{A}, P, R, \gamma)$, where \mathcal{S} is a finite set of states, \mathcal{A} is a finite set of actions, P is a state transition probability function, $P(s'|s, a)$, R is a reward function, $R(s, a)$ and $\gamma \in [0, 1]$ is a discount factor.

At each time step t , the agent observes the current state $s_t \in \mathcal{S}$ and chooses an action $a_t \in \mathcal{A}$. The environment then transitions to a new state s_{t+1} with probability $P(s_{t+1}|s_t, a_t)$ and the agent receives a reward $r_t = R(s_t, a_t)$. The goal of the agent is to find a policy $\pi : \mathcal{S} \rightarrow \mathcal{A}$ that maximizes the expected cumulative

discounted reward:

$$\max_{\pi} J^{\pi} = \mathbb{E}_{\pi, s_0 \sim \mu, s_{t+1} \sim P} \left[\sum_{t=0}^{\infty} \gamma^t R(s_t, \pi(s_t)) \right]$$

To do so, many algorithms were proposed in the literature varying in their assumptions on the problem, computational complexity and data requirements. Perhaps the most widely used algorithm today is PPO [28] which directly optimizes the policy using full trajectories while constraining it from diverging.

When the action space is high-dimensional, as in our case, learning becomes exponentially harder. This can lead to extremely slow learning progress, and requires function approximators [35], which are prone to overfitting and generalize poorly. Consequently, techniques specifically designed for high-dimensional action spaces, such as action abstraction, or dimensionality reduction [26], are often necessary to make the problem tractable and enable efficient reinforcement learning.

3 Method

We present RL-RC-DoT, an **RL**-based **Rate Controller for Downstream Task**, that dynamically optimizes macro-block QP deltas during video encoding. Simply put, our approach is to train a deep-RL agent that allocate bandwidth to different patches in each frame, only observing fast-to-compute features of every frame. To formalize the training framework, we cast the video compression problem with respect to a downstream task as a Markov decision process (MDP). In our formulation, each time-step of the MDP corresponds to processing one frame of the video. To train the policy, we use the PPO algorithm [28].

3.1 The MDP model

We now describe the various components of our model.

State space: We define the state of the environment to be per-patch statistics extracted from the encoder. The specific statistics we used are described below and in Appendix 7.1

Action space: We define an action to be a choice of all macro-block QP deltas within a frame. For example, given a frame resolution of 480x320 pixels parti-

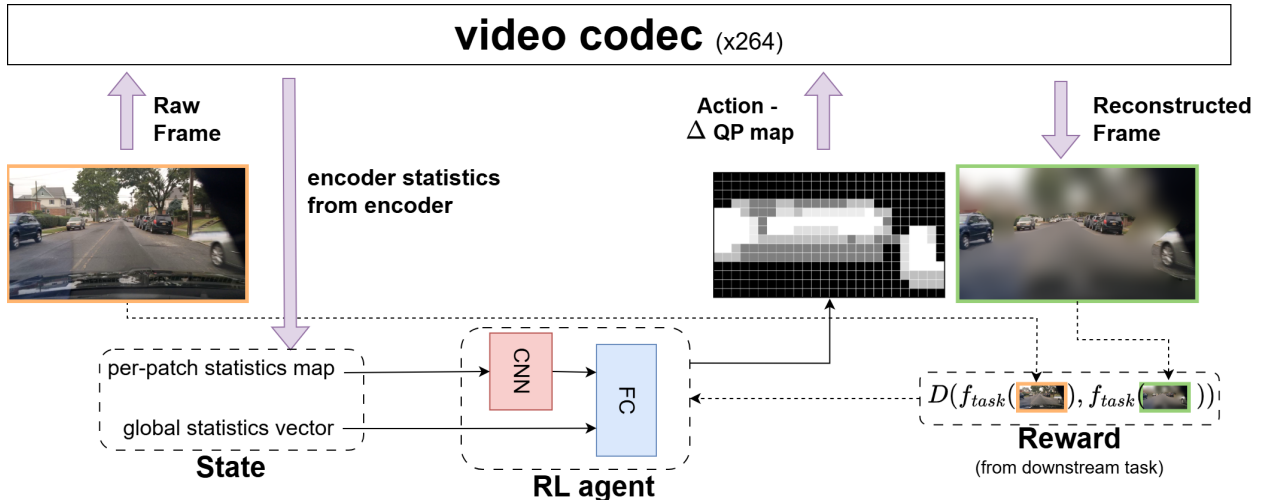


Figure 1: **RL-RC-DoT workflow.** Our proposed solution to the block-level control for a downstream task. RL-RC-DoT takes encoder statistics as input and outputs a block-level delta QP map. We then evaluate the difference in downstream task performance between the reconstructed frame and the raw frame. The reward contains both global score as reward and block-level score.

tioned into 16×16 pixel macro-blocks, the resulting action space constitutes a 30×20 dimensional matrix, where each value represent the delta between the frame level QP and the block specific QP. This action space is very high-dimensional and we discuss below an efficiency improvement.

Reward: We define the reward as a combination of two rewards with different purposes.

First, we wish to maximize the performance of the downstream task on decoded frames. Since ground-truth data is unavailable, we introduce a novel self-supervised approach. This method treats the downstream task’s output on the original uncompressed frame as a pseudo-ground-truth, against which we evaluate the task performance on the reconstructed frame:

$$r_{\text{task}} = D[f_{\text{task}}(\text{frame}_{\text{raw}}), f_{\text{task}}(\text{frame}_{\text{recon}})],$$

where f_{task} is a pre-trained model for the downstream-task and D is a task-specific objective function. For example, for car detection, f_{task} we use a pre-trained car detection model (YOLO-v5 nano [14]), and D measures how well the downstream task model of $f_{\text{task}}(\text{frame}_{\text{recon}})$ per-

forms compared to the raw data $f_{\text{task}}(\text{frame}_{\text{raw}})$. Here, $f_{\text{task}}(\text{frame}_{\text{raw}})$ is used as a pseudo-ground-truth, because we may not have access to the ground-truth of the frame.

The second component of the reward is designed for complying with the encoder’s bit-rate constraint. This is particularly crucial in streaming applications, where exceeding the allocated bandwidth can result in frame dropping and consequently deteriorate the viewer experience. The reward component $r_{\text{bit-rate}}$ for this objective is:

$$r_{\text{bit-rate}} = -\left| \log \left(\frac{\text{current average bit-rate}}{\text{target bit-rate}} \right) \right|.$$

The final reward is a weighted combination of the two components:

$$r = r_{\text{bit-rate}} + \lambda r_{\text{task}},$$

where λ is a hyper-parameter that determines rate-performance trade-off.

Efficient action space: The naive action space described above is very high dimensional, presenting a significant computational challenge in term of convergence

of reinforcement learning algorithms. To address this difficulty, we implement a coarsening approach: the agent operates on a lower-resolution action space, which is subsequently up-sampled to the original dimensions through interpolation. This technique facilitates more efficient training while maintaining the ability to generate fine-grained QP assignments. We analyze the impact of action space resolution on model performance in Appendix 7.5.

Finally, unlike previous approaches [18, 41] that relied on complex downstream task information (e.g. semantic maps, grad-cam), our method simplifies the state space by utilizing only encoder statistics that are readily available in the x264 encoder, so no additional calculations are required. A diagram of the full system is given in Figure 1 and additional details on the architecture used by the PPO algorithm is given in Appendix 7.2.

3.2 Macro-Block Reward Information

In most RL problems, the reward is a black-box directly mapping the state to a continuous score. Recent literature [42] has demonstrated that predictive modeling of rewards can significantly enhance agent performance. more specifically they implemented it as auxiliary heads alongside policy or value networks. In our setup, the reward presents a unique characteristic: the reward signals for various downstream tasks are often compositional. This occurs because the scores are derived from aggregating measurements across local patches in each input frame. For example, when optimizing for saliency-weighted PSNR, the reward is computed by aggregating per-pixel reconstruction errors.

To leverage this decomposable nature of rewards, we propose to add an auxiliary prediction loss for these sub-scores during back-propagation. Specifically, we introduce a block-wise loss that aims to predict for each individual block, the local reward that contribute to the overall task score. Adding this loss for macro-block level reward information is expected to enhance the agent’s performance, and for three reasons. First, it provides a more localized learning signal, allowing the agent to understand the impact of its actions on individual components of the reward. Second, by learning to predict these sub-scores, the agent develops a richer internal representation of the task structure. Lastly, this method aligns the agent’s learning more closely with the actual composition of the re-

ward, potentially leading to faster convergence and more stable learning. Section 5.4 shows the effect of this improvement.

4 Experiments

We evaluate our approach with two downstream tasks: car detection and region-of-interest (ROI) encoding [20]. We further study the robustness of the method, when a trained compression policy is tested with a different car detector, or even in a segmentation task instead of detection. Finally, we report performance of ablation experiments.

4.1 Dataset

We trained and evaluated RL-RC-DoT using a subset of video streams from the BDD100K dataset [43], a large-scale driving video dataset, with multi-task annotations. We reconstructed the raw data from the videos and to allow faster training time, we resized them to a smaller resolution of 480x320 pixels. We then filtered out streams that exhibited trivial rate-task performance (RD) curves with respect to the downstream tasks of car detection precision, when encoded with the standard x264 codec [38]. We specifically excluded streams that showed zero precision across most target bit-rates. This approach ensured that our dataset presented meaningful challenges for compression optimization.

Our final dataset comprised of 172 streams in total, with 65 streams used for training our agent, 7 streams used for evaluation on different hyper-parameters and 100 streams reserved for testing. For reproducibility, we provided a detailed list of the specific stream used in our experiments in appendix 7.6 of this paper.

4.2 Evaluation metrics: RD-curve and BD-rate

Since compression is a constraint optimization problem, it is standard to depict results using a Rate-Distortion (RD) curve. An RD-curve illustrates the trade-off between bit-rate constraint and quality in video compression (see examples in Figure 2). RD-curves are traditionally used with PSNR, but are equally applicable to task-specific metrics like precision/recall for a detection task or

	Precision		Recall		PSNR	
	low-rate	high-rate	low-rate	high-rate	low-rate	high-rate
x264	.22 ± .0013	.66 ± .0015	.45 ± .002	.81 ± .001	28.98 ± .03	34.55 ± .03
RL-RC-DoT(ours)	.36 ± .0015	.71 ± .0014	.63 ± .002	.83 ± .001	29.03 ± .03	34.55 ± .03

Table 1: Car detection precision and recall of YOLO5, and PSNR. Value are mean and s.e.m. calculated across all frames from a test set of 100 videos from BDD100K.

saliency-weighted PSNR for ROI-based encoding. These RD-curves allow us to evaluate compression efficiency for any downstream tasks on reconstructed videos.

BD-rate (Bjontegaard Delta rate; [2]) is a widely used metric in video compression to compare the efficiency of different encoding methods. This method calculates the average difference in bit-rate between two rate-distortion (RD) curves at the same quality level. The BD-rate represents the percentage of bit-rate savings that one encoding method achieves over another while maintaining equivalent video quality performance. Thus, a negative BD-rate indicates that the test method requires less bits than the reference method to achieve the same quality / task performance.

4.3 Compared methods:

To conduct a fair and meaningful comparison against existing baselines, they should be solving the same task, and particularly have access to the same information. Several previous studies developed methods for task-aware encoding, but their setup is fundamentally different. For instance, some previous methods assume access to the downstream model during inference [41] resulting in a much higher computational cost depending on the task. [18] and [8] focus on a single-frame (image) compression, ignoring the overall video budget constraints. Finally, most methods did not release code [8, 29]. These differences in approach and constraints make direct comparisons misleading.

4.4 Experimental details

All of our experiments use the x264 open source encoder software [25], with the *medium* preset and target bit-rates 50 – 200 kbps. To extract the statistics we allow x264 to use look-ahead for 10 frames. For car detection,

we employ YOLOv5-nano [14]. ROI encoding is evaluated using saliency maps generated by TranSalNet [21]. Our agent is trained using Stable-Baselines3 [27] implemented PPO with the reward function described in Section 3. We augment the standard PPO algorithm with a reward per block prediction network, as described in Section 3.2. To facilitate efficient training, we utilize 8 parallel environments running on an Intel(R) Xeon(R) CPU E5-2698 v4 @ 2.20GHz, complemented by an NVIDIA Tesla V100 32GB GPU. Each agent undergoes training on 20 million frames, a process that spans approximately 4 days. Our training achieves a frame rate of roughly 50 FPS, while evaluation in a single environment maintains around 30 FPS, demonstrating the feasibility of real-time streaming applications.

5 Results

5.1 Car Detection

We first assess the performance of RL-RC-DoT in the context of video compression optimized for car detection. The reward function for training our RL agent is based on the precision score of YOLOv5-nano [14]. In practice it was calculated as true positives divided by total positives in the granularity of the detection boxes. For our additional auxiliary loss described in Section 3.2, we compute the precision score for each individual block separately to generate block-specific reward information. We report the policy’s performance on 100 test videos from the BDD100K dataset.

Table 1 compares RL-RC-DoT with the standard x264 encoder, focusing on the detection performance of the YOLOv5-nano detector on compressed videos. The evaluation is conducted across multiple compression rates, with results averaged over all frames in the test dataset for

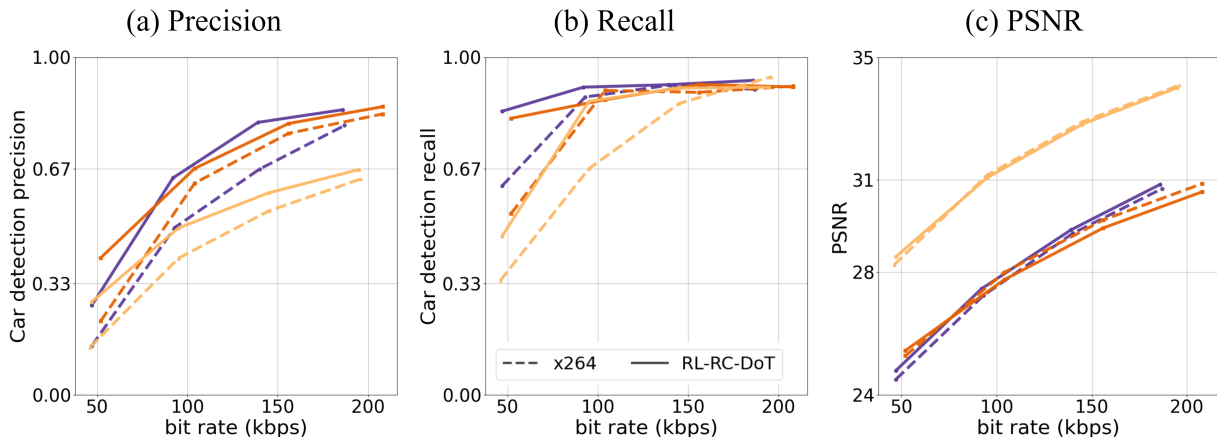


Figure 2: Rate-Quality curves for Car detection task. Comparing standard x264 (dashed lines) with RL-RC-DoT (solid lines). Curves show three example streams, demonstrating how RL-RC-DoT improves quality across the range of bit-rate values. (a) Car detection precision (b) recall (c) PSNR.

each target bit-rate. We also applied the same comparative approach to assess the PSNR of the reconstructed streams. The results demonstrating that RL-RC-DoT improves car detection precision and recall significantly, with minimal impact on the PSNR of the compressed videos.

Figure 2 illustrates the superiority of RL-RC-DoT over the standard x264 encoder through RD curves for three representative video streams. Figure 3, shows a qualitative example of the performance gain. We compare the images in both types of rate-control, and the output of the downstream task. We can see the details corresponding to the downstream task are better reconstructed yielding a more relevant image.

To quantify the performance difference between methods, we compute the BD-rate (see 4.2), a standard metric in the field. Our approach shows significant improvements in detection performance, with BD-rate reductions of $24.7\%(\pm 1.38\%)$. These gains come at a minimal cost to overall video quality, yielding a slight increase (deterioration) in PSNR BD-rate of $1.19\%(\pm 0.46\%)$ (Table 2). This means that videos compressed using RL-RC-DoT remains understandable to human viewers, a crucial aspect for validation and debug purposes. It also exhibits robustness to different task models, which we elaborate on in section 5.3.

5.2 ROI encoding

We conducted similar experiments for ROI-encoding task by promoting saliency weighted PSNR as the task score. RL-RC-DoT exhibits a BD-rate value of $-25.64\%(\pm 0.99\%)$, indicating that our method achieves significantly better quality in salient regions at lower bit-rates compared to x264. Interestingly, the PSNR BD-rate obtained is -5.26 ± 0.36 which is slightly better than the vanilla rate-control. This may be due to the proximity between the two tasks. This also shows the sub-optimality of the vanilla rate-control when considering specific content. Figure 4 illustrates the RD curves for three representative video streams. These curves demonstrate that in most cases, RL-RC-DoT achieves a more favorable RD trade-off for ROI encoding task compared to x264. Figure 5 provides qualitative examples of our method’s performance, visually illustrating the enhanced quality in salient regions compared to the baseline encoding.

5.3 Task Robustness

An important concern is that RL-RC-DoT might overfit for the training task. That would mean that changing the model, may harshly hurt performance. We set to evalu-

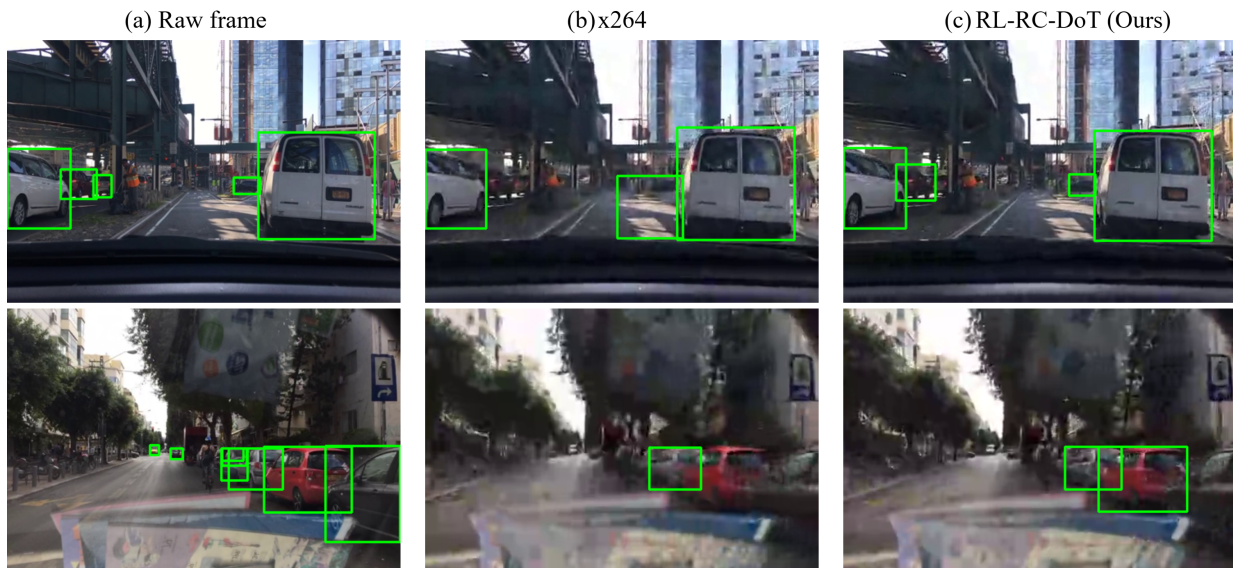


Figure 3: Car detection example result. (a) detection output on x264 reconstructed frame, (b) output on raw frame and (c) output on RL-RC-DoT reconstructed frame. Notice that both RL-RC-DoT and x264 used the same target bit-rate

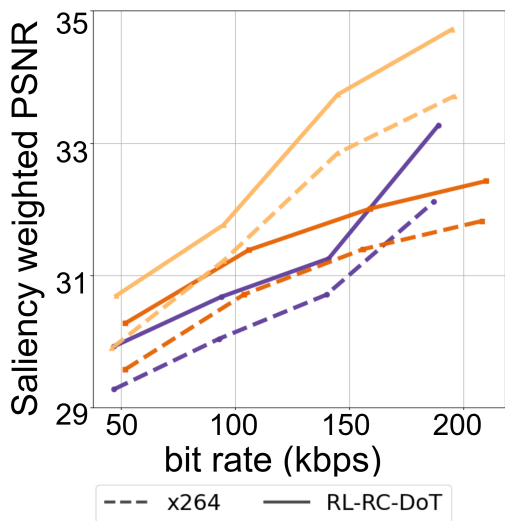


Figure 4: RD-curves for 3 videos for ROI-encoding.

ate robustness to such changes in RL-RC-DoT by training the policy with one downstream task, and testing it with another. More specifically, we optimized the policy for car detection using the YOLOv5-nano model, as described in section 5.1. Then, we measured the detection performance of another model, SSD [19]. We also measure the performance on the related but distinct task of car segmentation (DeepLab; [6]). The results are also listed in Table 2.

Precision (YOLO)	Recall (YOLO)	PSNR
-24.7 ± 1.57	-19.75 ± 2.97	1.19 ± 0.46
Precision (SSD)	Recall (SSD)	Segmentation IOU
-26.2 ± 1.48	-25.81 ± 2.03	-14.6 ± 1.81

Table 2: BD-rate Results on RL-RC-DoT applied on test set for the car detection task for various settings. Negative values mean that RL-RC-DoT improves over baseline.

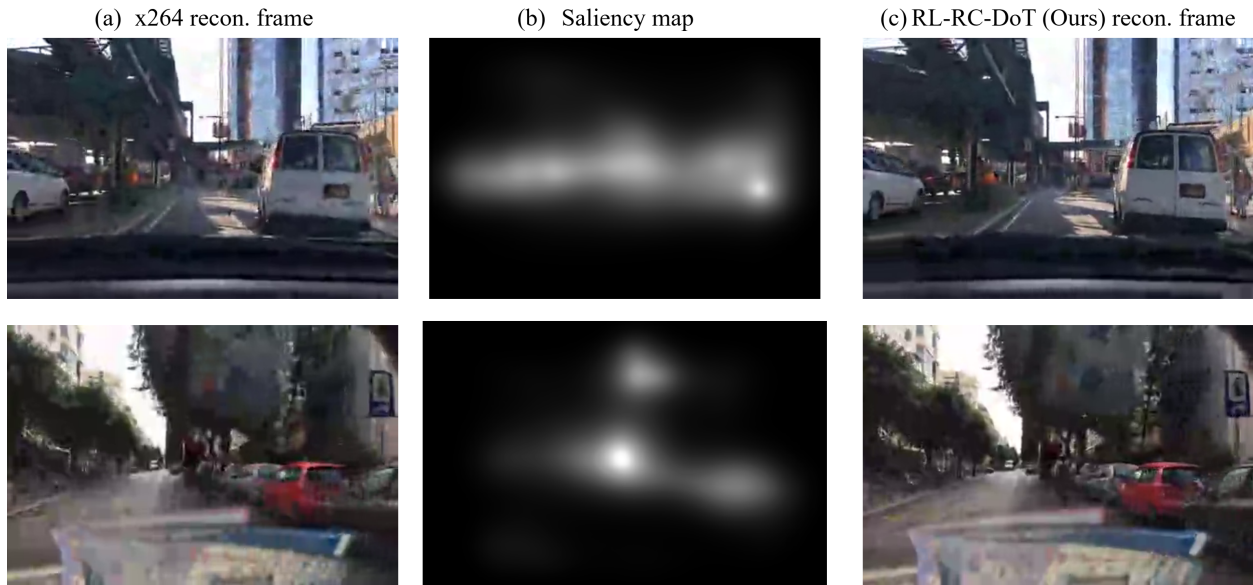


Figure 5: Saliency weighted PSNR results. (a) x264 reconstructed frame, (b) Saliency map of raw frame, extracted with [21] (c) RL-RC-DoT reconstructed frame. Notice that both RL-RC-DoT and x264 used the same target bit-rate

This approach allows us to examine whether our method truly captures fundamental aspects of visual information relevant to automotive perception tasks, rather than overfitting to a specific model or narrow task definition. By demonstrating performance improvements across different models and related tasks, we aim to show that our compression method preserves task-relevant information in a more general sense, potentially allowing for model updates or task modifications without the need to retrain the compression policy. This robustness is crucial for real-world applications where deployed systems may need to adapt to new models or slightly different tasks over time.

For car detection evaluated with SSD, the precision BD-rate is very similar to precision with YOLOv5-nano, which was used for training. For car segmentation, although tested with a different task, we still observe an improved but weaker BD-rate than the detection task. This improvement can be attributed to the close relation between the tasks, so meaningful macro-blocks for car detection, are also useful for the segmentation task. In sum-

mary, the BD-rate obtained on the PSNR and the various tasks show the robustness of our method to new tasks and new models that solve the task. Additional qualitative experiments examining task robustness are detailed in the appendix

5.4 Ablation Experiments

To quantify the relative contribution of various components of our method, we perform ablation studies, for both car detection and ROI encoding, and provide the results in Table 3. For both tasks, we first ablated the macro-block reward information as described in Subsection 3.2. Then, ran an experiment for $\gamma = 0$ which shows what happens when optimizing for a myopic policy.

The results show that reward info improved the learning process and reduces the BD-rate even further for both tasks. This demonstrates the benefit of exploiting additional information in the video compression domain that is generally not available. For $\gamma = 0$, the BD-rate is significantly worse for both tasks. As expected, ignoring the future implications of the bit-allocation can cause

Car detection	Precision BD-rate	PSNR BD-rate
RL-RC-DoT	-24.7 ± 1.57	1.19 ± 0.46
RL-RC-DoT w/o RI	-19.4 ± 1.38	1.92 ± 0.41
RL-RC-DoT $\gamma = 0$	-9.78 ± 1.29	5.44 ± 0.6

ROI encoding	Sal.-weighted PSNR BD-rate	PSNR BD-rate
RL-RC-DoT	-25.64 ± 0.99	-5.26 ± 0.36
RL-RC-DoT w/o RI	-23.46 ± 0.97	-4.54 ± 0.42
RL-RC-DoT $\gamma = 0$	-16.01 ± 0.77	2.11 ± 0.31

Table 3: Ablation study. (1) Full RL-RC-DoT (2) Omitting reward information (RI) from the training process and (3) Ignoring long term effects by using a myopic policy.

sub-optimal decisions for the entire video. This also emphasizes the limitation of rate-control methods optimizing for every frame separately; a common practice by previous works.

6 Conclusions and Limitations

Machine learning for videos understanding became prevalent in numerous applications, but impose high costs of storing, making fast encoding and low bit-rate critical. Task-aware compression has huge potential, but existing methods have critical limitations, like heavy compute or dependency on ground truth task data for compression. We develop an efficient RL solution which encodes every frame in real time while optimizing the future bit-rate and task performance on the reconstructed video. Our learned policy is robust against changes in the downstream models for the same task and to closely related tasks, showing large important potential for data collection for autonomous vehicle, patient monitoring and robotics.

Limitations: Training our models involves encoding and performing the downstream task per frame, and this may slow down converge depending on the complexity of the downstream task. Also, generalizing across video resolutions may be hard because it affects the size of action space and the complexity of the learning problem.

References

- [1] BHASKARAN, V., AND KONSTANTINIDES, K. Image and video compression standards: algorithms and architectures. **1**
- [2] BJØNTEGAARD, G. Calculation of average psnr differences between rd-curves. **7**
- [3] BROSS, B., WANG, Y.-K., YE, Y., LIU, S., CHEN, J., SULLIVAN, G. J., AND OHM, J.-R. Overview of the versatile video coding (vvc) standard and its applications. IEEE Transactions on Circuits and Systems for Video Technology **31**, 10 (2021), 3736–3764. **1**
- [4] CAI, Q., CHEN, Z., WU, D. O., LIU, S., AND LI, X. A novel video coding strategy in hevc for object detection. IEEE Transactions on Circuits and Systems for Video Technology **31**, 12 (2021), 4924–4937. **3**
- [5] CHEN, L.-C., HU, J.-H., AND PENG, W.-H. Reinforcement learning for hevc/h. 265 frame-level bit allocation. In 2018 IEEE 23rd International Conference on Digital Signal Processing (DSP) (2018), IEEE, pp. 1–5. **2**
- [6] CHEN, L.-C., PAPANDREOU, G., KOKKINOS, I., MURPHY, K., AND YUILLE, A. L. Deeplab: Semantic image segmentation with deep convolutional nets, atrous convolution, and fully connected crfs. IEEE transactions on pattern analysis and machine intelligence **40**, 4 (2017), 834–848. **9**
- [7] ELGAMAL, T., SHI, S., GUPTA, V., JANA, R., AND NAHRSTEDT, K. Sieve: Semantically encoded video analytics on edge and cloud. In 2020 IEEE 40th International Conference on Distributed Computing Systems (ICDCS) (2020), IEEE, pp. 1383–1388. **2**
- [8] FISCHER, K., BRAND, F., HERGLOTZ, C., AND KAUP, A. Video coding for machines with feature-based rate-distortion optimization. In 2020 IEEE 22nd International Workshop on Multimedia Signal Processing (MMSP) (2020), IEEE, pp. 1–6. **3, 7**
- [9] GALTERI, L., BERTINI, M., SEIDENARI, L., AND DEL BIMBO, A. Video compression for object detection algorithms. In 2018 24th International Conference on Pattern Recognition (ICPR) (2018), IEEE, pp. 3007–3012. **3**
- [10] GE, X., LUO, J., ZHANG, X., XU, T., LU, G., HE, D., GENG, J., WANG, Y., ZHANG, J., AND QIN, H. Task-aware encoder control for deep video compression. In Proceedings of the IEEE/CVF Conference on Computer Vision and Pattern Recognition (2024), pp. 26036–26045. **2**
- [11] HO, Y.-H., JIN, G.-L., LIANG, Y., PENG, W.-H., AND LI, X. A dual-critic reinforcement learning framework for frame-level bit allocation in hevc/h. 265. In 2021 Data compression conference (DCC) (2021), IEEE, pp. 13–22. **2**
- [12] HO, Y.-H., KAO, C.-H., PENG, W.-H., AND HSIEH, P.-C. Neural frank-wolfe policy optimization for region-of-interest intra-frame coding with hevc/h. 265. In 2022 IEEE International Conference on Visual Communications and Image Processing (VCIP) (2022), IEEE, pp. 1–5. **2**
- [13] HU, J.-H., PENG, W.-H., AND CHUNG, C.-H. Reinforcement learning for hevc/h. 265 intra-frame rate control. In 2018 IEEE International Symposium on Circuits and Systems (ISCAS) (2018), IEEE, pp. 1–5. **2**
- [14] JOCHER, G. ultralytics/yolov5. <https://github.com/ultralytics/ultralytics>, Oct. 2020. **5, 7**
- [15] KONG, L., DAI, R., AND ZHANG, Y. A new quality model for object detection using compressed videos. In 2016 IEEE International Conference on Image Processing (ICIP) (2016), IEEE, pp. 3797–3801. **4**
- [16] KUFA, J., AND KRATOCHVIL, T. Software and hardware hevc encoding. In 2017 International Conference on Systems, Signals and Image Processing (IWSSIP) (2017), IEEE, pp. 1–5. **1**
- [17] LI, P.-H., ANKIREDDY, S. K., ZHAO, R. P., NOURKHIZ MAHJOUN, H., MORADI PARI, E., TOPCU, U., CHINCHALI, S., AND KIM, H. Task-aware distributed source coding under dynamic bandwidth. Advances in Neural Information Processing Systems **36** (2024). **2**
- [18] LI, X., SHI, J., AND CHEN, Z. Task-driven semantic coding via reinforcement learning. IEEE Transactions on Image Processing **30** (2021), 6307–6320. **2, 3, 6, 7**
- [19] LIU, W., ANGUELOV, D., ERHAN, D., SZEGEDY, C., REED, S., FU, C.-Y., AND BERG, A. C. Ssd: Single shot multibox detector. In Computer Vision—ECCV 2016: 14th European Conference, Amsterdam, The Netherlands, October 11–14, 2016, Proceedings, Part I **14** (2016), Springer, pp. 21–37. **9**

- [20] LIU, Y., LI, Z. G., AND SOH, Y. C. Region-of-interest based resource allocation for conversational video communication of h. 264/avc. IEEE transactions on circuits and systems for video technology 18, 1 (2008), 134–139. 6
- [21] LOU, J., LIN, H., MARSHALL, D., SAUPE, D., AND LIU, H. Transalnet: Towards perceptually relevant visual saliency prediction. Neurocomputing (2022). 7, 10, 9
- [22] LU, G., OUYANG, W., XU, D., ZHANG, X., CAI, C., AND GAO, Z. Dvc: An end-to-end deep video compression framework. In Proceedings of the IEEE/CVF conference on computer vision and pattern recognition (2019), pp. 11006–11015. 2
- [23] MANDHANE, A., ZHERNOV, A., RAUH, M., GU, C., WANG, M., XUE, F., SHANG, W., PANG, D., CLAUS, R., CHIANG, C.-H., ET AL. Muzero with self-competition for rate control in vp9 video compression. arXiv preprint arXiv:2202.06626 (2022). 2
- [24] MAO, H., GU, C., WANG, M., CHEN, A., LAZIC, N., LEVINE, N., PANG, D., CLAUS, R., HECHTMAN, M., CHIANG, C.-H., ET AL. Neural rate control for video encoding using imitation learning. arXiv preprint arXiv:2012.05339 (2020). 2
- [25] MERRITT, L., AND VANAM, R. x264: A high performance h. 264/avc encoder. online] http://neuron2.net/library/avc/overview_x264.v8.5.pdf (2006). 2, 3, 7
- [26] PIERROT, T., MACÉ, V., SEVESTRE, J.-B., MONIER, L., LATERRE, A., PERRIN, N., BEGUIR, K., AND SIGAUD, O. Factored action spaces in deep reinforcement learning. 4
- [27] RAFFIN, A., HILL, A., GLEAVE, A., KANERVISTO, A., ERNESTUS, M., AND DORMANN, N. Stable-baselines3: Reliable reinforcement learning implementations. Journal of Machine Learning Research 22, 268 (2021), 1–8. 7
- [28] SCHULMAN, J., WOLSKI, F., DHARIWAL, P., RADFORD, A., AND KLIMOV, O. Proximal policy optimization algorithms. arXiv preprint arXiv:1707.06347 (2017). 4, 2
- [29] SHI, J., AND CHEN, Z. Reinforced bit allocation under task-driven semantic distortion metrics. In 2020 IEEE international symposium on circuits and systems (ISCAS) (2020), IEEE, pp. 1–5. 2, 4, 7
- [30] SHOR, J., AND JOHNSTON, N. The need for medically aware video compression in gastroenterology. arXiv preprint arXiv:2211.01472 (2022). 2
- [31] SINGH, P., DELP, E. J., AND REIBMAN, A. R. Video-analytics task-aware quad-tree partitioning and quantization for hevc. In 2022 IEEE International Conference on Image Processing (ICIP) (2022), IEEE, pp. 2936–2940. 3
- [32] SULLIVAN, G. J., OHM, J.-R., HAN, W.-J., AND WIEGAND, T. Overview of the high efficiency video coding (hevc) standard. IEEE Transactions on circuits and systems for video technology 22, 12 (2012), 1649–1668. 1, 2
- [33] SUTTON, R. S., AND BARTO, A. G. Reinforcement Learning: An Introduction. The MIT Press, Cambridge, MA, 1998. 4
- [34] TOMAR, S. Converting video formats with ffmpeg. Linux Journal 2006, 146 (2006), 10. 7
- [35] VAN HASSELT, H., AND WIERING, M. A. Reinforcement learning in continuous action spaces. In 2007 IEEE International Symposium on Approximate Dynamic Programming and Reinforcement Learning (2007), IEEE, pp. 272–279. 4
- [36] WANG, Z., BOVIK, A. C., SHEIKH, H. R., AND SIMONCELLI, E. P. Image quality assessment: from error visibility to structural similarity. IEEE transactions on image processing 13, 4 (2004), 600–612. 3
- [37] WENGER, S. H. 264/avc over ip. IEEE transactions on circuits and systems for video technology 13, 7 (2003), 645–656. 1
- [38] WIEGAND, T., SULLIVAN, G. J., BJONTEGAARD, G., AND LUTHRA, A. Overview of the h. 264/avc video coding standard. IEEE Transactions on circuits and systems for video technology 13, 7 (2003), 560–576. 3, 6
- [39] WINDSHEIMER, M., BRAND, F., AND KAUP, A. On annotation-free optimization of video coding for machines. arXiv preprint arXiv:2406.07938 (2024). 3
- [40] WU, C., QUAN, G., HE, G., LAI, X.-Q., LI, Y., YU, W., LIN, X., AND YANG, C. Qs-nerv: Real-time quality-scalable decoding with neural representation for videos. In ACM Multimedia 2024 (2024). 3
- [41] XIE, G., LI, X., LIN, S., CHEN, Z., ZHANG, L., ZHANG, K., AND LI, Y. Hierarchical reinforcement learning based video semantic coding for segmentation. In 2022 IEEE International Conference on Visual Communications and Image Processing (VCIP) (2022), IEEE, pp. 1–5. 2, 3, 6, 7

- [42] YE, W., LIU, S., KURUTACH, T., ABBEEL, P., AND GAO, Y. Mastering atari games with limited data. Advances in neural information processing systems 34 (2021), 25476–25488. 6
- [43] YU, F., CHEN, H., WANG, X., XIAN, W., CHEN, Y., LIU, F., MADHAVAN, V., AND DARRELL, T. Bdd100k: A diverse driving dataset for heterogeneous multitask learning. In Proceedings of the IEEE/CVF conference on computer vision and pattern recognition (2020), pp. 2636–2645. 6, 7
- [44] ZHANG, H., AHONEN, J. I., LE, N., YANG, R., AND CRICRI, F. Competitive learning for achieving content-specific filters in video coding for machines. arXiv preprint arXiv:2406.12367 (2024). 2

7 Appendix

7.1 Environment details

Global encoder statistics used as state information
Next frame x264 selected QP value
Next frame number
Current bitstream size
Current frame x264 selected QP value
Average QP
Percentages of I type Macro Blocks
Percentages of P type Macro Blocks
Percentages of skip-type Macro Blocks
x264 calculated PSNR
x264 calculated SSIM
Percentages of bits used for Motion Vectors
Percentages of bits used for DCT coefficient
Progress of encoding
bit-rate error
Next frame type
Next frame complexity

Table 4: Detailed components of global encoder statistic used in state information

Local (per-MB) encoder statistic used as state information
x264 energy values per Macro Block
x264 intra encoding cost per Macro Block
x264 propagating encoding cost per Macro Block
x264 inverse quantization scale factor per Macro Block

Table 5: Detailed components of per-MB encoder statistic used in state information

7.2 Agent architecture

To train the policy, we use the PPO algorithm [28], where the architecture of the policy is as follows: The per-block statistics are processed through a compact convolutional neural network (CNN) comprising three convolutional layers. These layers employ kernel sizes of 3×3 or 4×4 with a stride of 1. The resulting features are subsequently flattened and concatenated with the global statistics. A fully connected layer then derives a latent representation of dimension 64. This latent representation serves as input to three distinct fully connected networks: the value network (critic), the policy network (actor), and the reward prediction network described in the following subsection. A diagram of the full system is given in Figure 6. The agent’s stochastic policy is modeled using a diagonal multivariate Gaussian distribution, where the agent learns the state-dependent mean vectors while maintaining independent standard deviation parameters for each dimension.

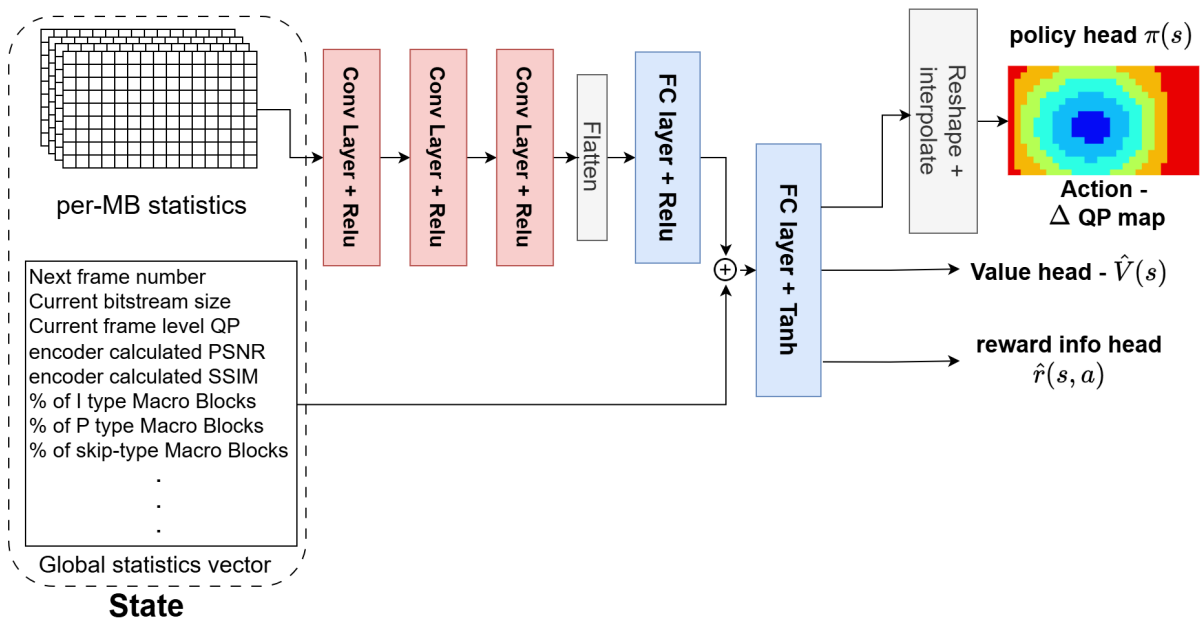


Figure 6: RL-RC-DoT agent architecture; Input is the statistics from the encoder, the output is the delta QP map

7.3 Further results

Full results tables with bit-rate error: Here, we provide all of the tables used in the main text with the bit-rate error data.

ROI encoding experiment	Saliency-weighted PSNR BD-rate	PSNR BD-rate	Bit-rate error [$1e - 3$]
RL-RC-DoT	-25.64 ± 0.99	-5.26 ± 0.36	-1.0 ± 0.43

Table 6: Results on RL-RC-DoT applied on the test-set for the saliency-weighted PSNR task.

	Precision (YOLO)	Recall (YOLO)	PSNR	Precision (SSD)
RL-RC-DoT	-24.7 ± 1.57	-19.75 ± 2.97	1.19 ± 0.46	-26.2 ± 1.48
	Recall (SSD)	Segmentation IOU	Bit-rate error [$1e - 3$]	
RL-RC-DoT	-25.81 ± 2.03	-14.6 ± 1.81	0.13 ± 0.44	

Table 7: BD-rate Results on RL-RC-DoT applied on test set for the car detection task for various settings. Negative values mean that RL-RC-DoT improves over baseline.

Car detection	Precision BD-rate	Recall BD-rate	PSNR BD-rate	Bit-rate error [$1e - 3$]
RL-RC-DoT	-24.7 ± 1.57	-19.75 ± 2.97	1.19 ± 0.46	0.13 ± 0.44
RL-RC-DoT w/o RI	-19.4 ± 1.38	-11.94 ± 1.7	1.92 ± 0.41	0.4 ± 0.47
RL-RC-DoT $\gamma = 0$	-9.78 ± 1.29	-10.28 ± 2.14	5.44 ± 0.6	2.4 ± 0.44
ROI encoding	Saliency-weighted PSNR BD-rate	PSNR BD-rate	Bit-rate error [$1e - 3$]	
RL-RC-DoT	-25.64 ± 0.99	-5.26 ± 0.36	-1.0 ± 0.43	
RL-RC-DoT w/o RI	-23.46 ± 0.97	-4.54 ± 0.42	5.3 ± 0.48	
RL-RC-DoT $\gamma = 0$	-16.01 ± 0.77	2.11 ± 0.31	6.9 ± 0.43	

Table 8: Ablation study. (1) Full RL-RC-DoT (2) Omitting reward information (RI) from the training process and (3) Ignoring long term effects by using a myopic policy.

Here we give more qualitative results, Figures 8 and 8 gives more detection comparison between RL-RC-DoT and x264.

Qualitative results on task-robustness: Figure 9, shows a qualitative example of task robustness. We compare the images in both types of rate-control, and the output of the downstream task. We can see the details corresponding to the downstream task are better reconstructed yielding a more relevant image.

7.4 Task accuracy to distortion trade-off

As previously discussed, RL-RC-DoT gains BD-rate reductions of $24.7\%(\pm 1.38\%)$ with respect to car detection precision task, while paying a minimal cost to overall video quality, as evidenced by a slight increase in PSNR BD-rate of $1.19\%(0.46\%)$. This is important since we want video to still be watchable by human eyes, for validation purposes and robustness to changing task models.

To further illustrate this point, in Figure 10 we show the PSNR and task performance BD-rate obtained by RL-RC-DoT for each stream in the test set. In the plots we see the PSNR varies around 0 while the tasks performance is well below.

7.5 Action Space Resolution

Since we show our results on a videos of size 480x320 with macro-blocks of size 16x16, the action space is of size 30x20. The size of the action space drastically affects the performance of the agent and the convergence rate of the training process. Thus, we propose to set a lower resolution action space and upsample to the original action space by interpolation. The trade-off here is clear – if we make decisions in high resolution, the agent can take a long time to converge, whereas a low resolution decision will not provide the finer control required for accurate bit allocation for the downstream-task resulting in a sub-optimal performance. We illustrate this notion in Figure 11. We plot the task BD-rate for multiple choices of resolution reduction ratios for each of the tasks. The plot indeed shows the trade-off between the two, where each task has a different optimal choice for action space resolution. We note that these results may depend on the number of frames allotted for training, where we expect longer training to benefit lower resolutions.

7.6 BDD100K streams

Here we elaborate on the streams we used from bdd100k dataset [43]:

7.7 Reproducibility of experiments

Encoder environment: To apply rate-control on the environment we changed the code of the open source x264 [25] encoder so that in each frame it can obtain delta-QP values externally and provide relevant statistics as described in Appendix 7.1.

RL Agent: We provide a description of the policy’s architecture in Appendix 7.2. The agent was trained using PPO implementation from stable-baselines3 [27] with default parameters, where we just added an MSE prediction loss (with weight 0.1) for reward info. We used $\lambda = 20$ to average between the bit-rate and downstream task rewards.

Experiments: In our experiments we used the publicly available BDD100K dataset (4.1) which was resized using the open source package ffmpeg[34]. We provide the named list of streams we used in Appendix 7.6. In the experimental details subsection 4.4 we provide additional information on the hardware we used and the downstream task models we used for our experiments.



Figure 7: Car detection example result. (a) detection output on x264 reconstructed frame, (b) output on raw frame and (c) output on RL-RC-DoT reconstructed frame. Notice that both RL-RC-DoT and x264 used the same target bit-rate

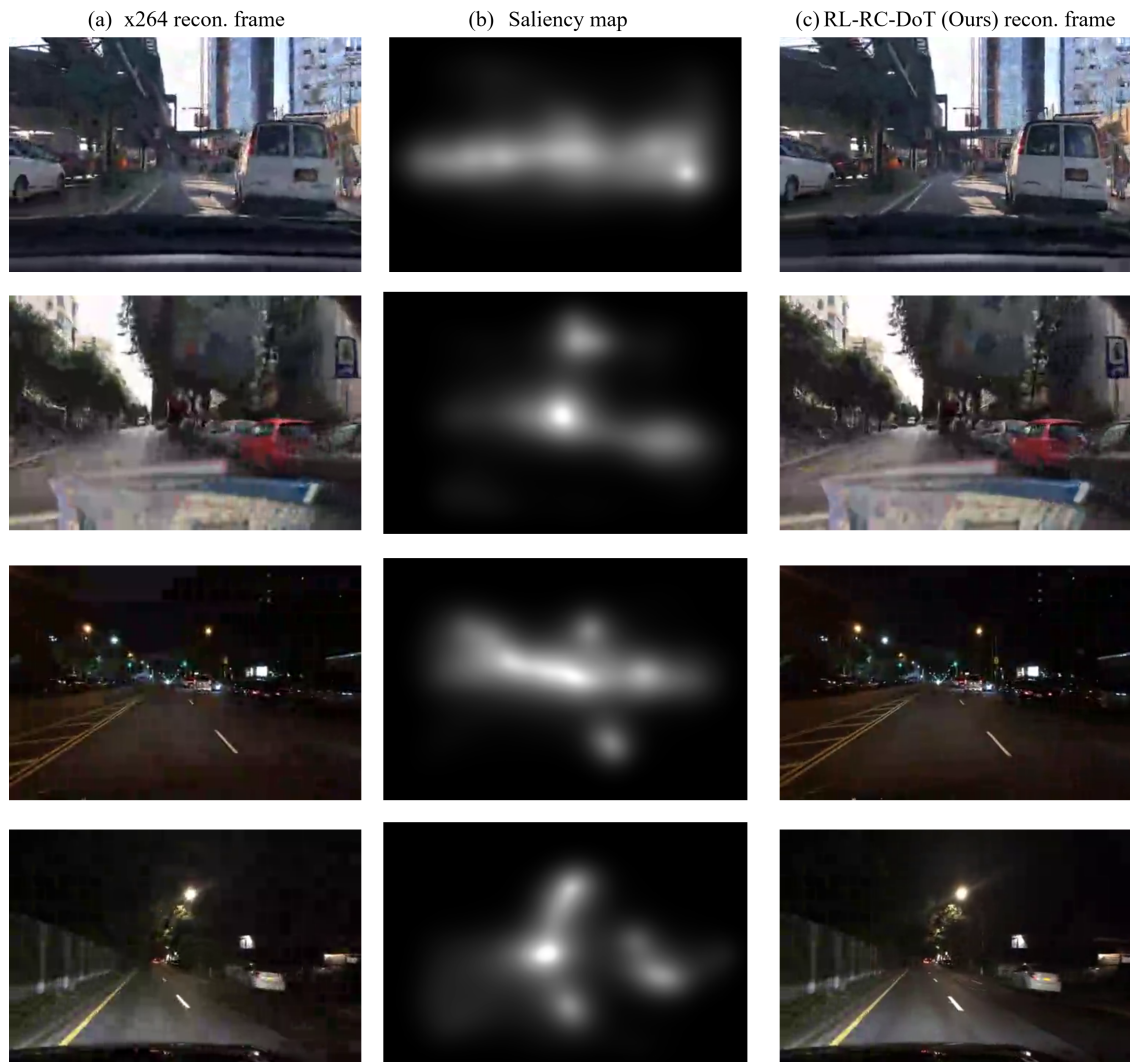


Figure 8: Saliency weighted PSNR results. (a) x264 reconstructed frame, (b) Saliency map of raw frame, extracted with [21] (c) RL-RC-DoT reconstructed frame. Notice that both RL-RC-DoT and x264 used the same target bit-rate

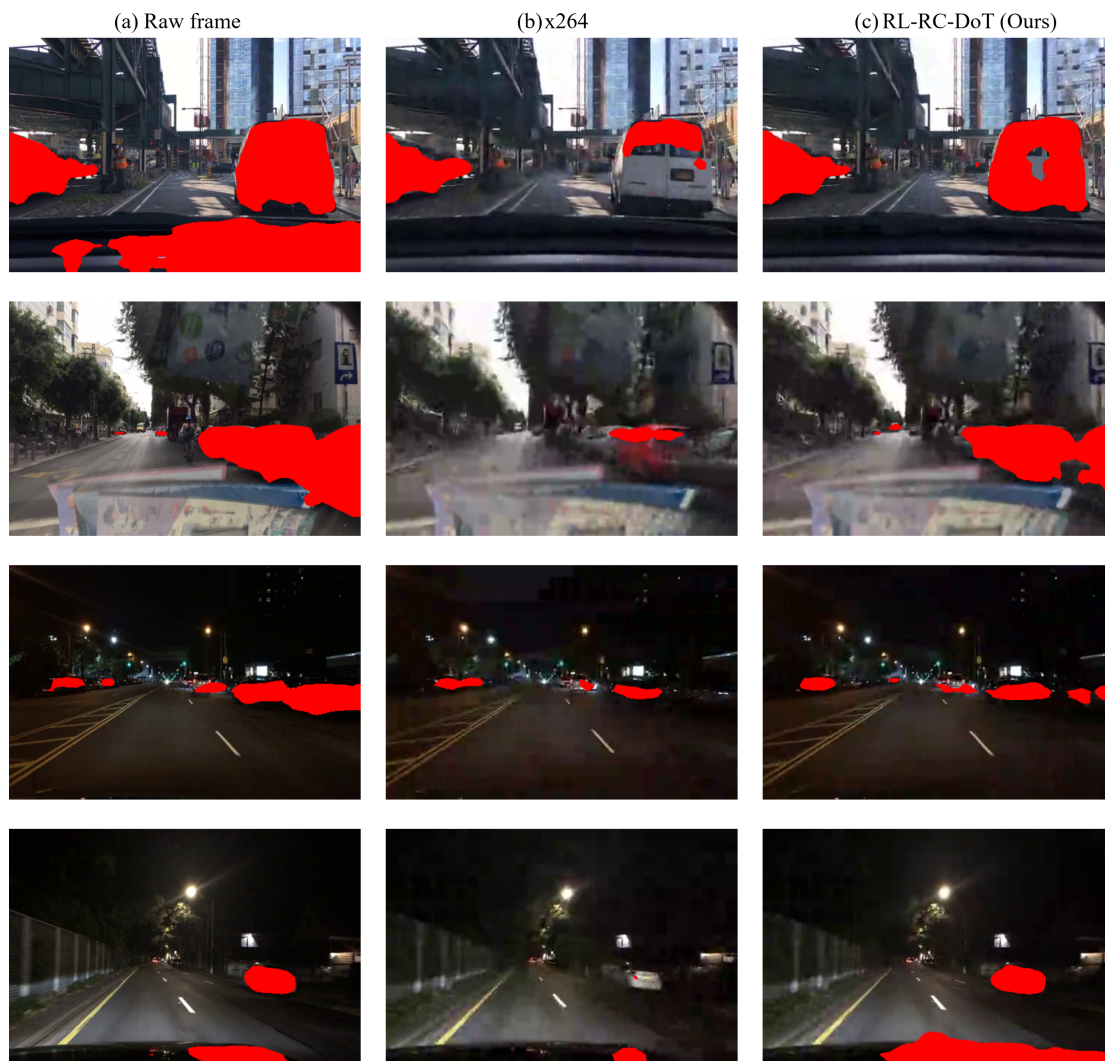


Figure 9: Car segmentation result comparison. (a) segmentation output on x264 reconstructed frame, (b) output on raw frame and (c) output on RL-RC-DoT reconstructed frame. Notice that both RL-RC-DoT and x264 used the same target bit-rate

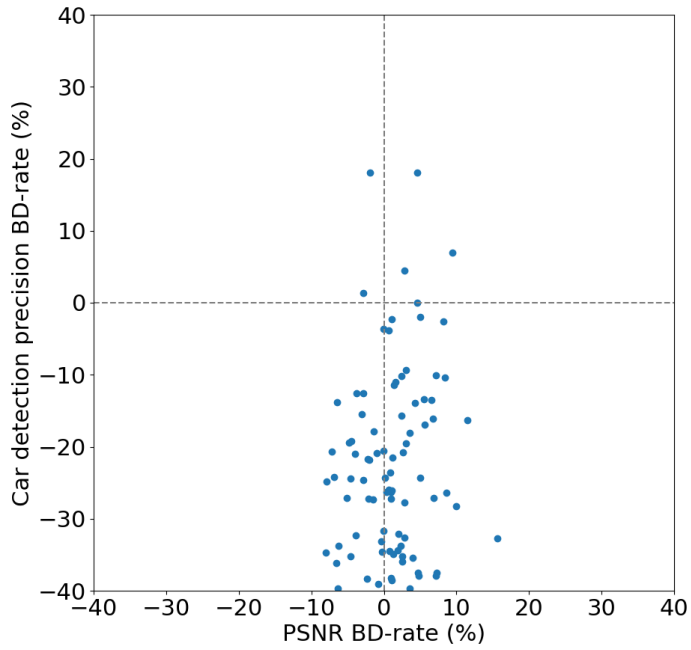


Figure 10: PSNR BD-rate to detection precision BD-rate, where each point represent a single stream in the test set

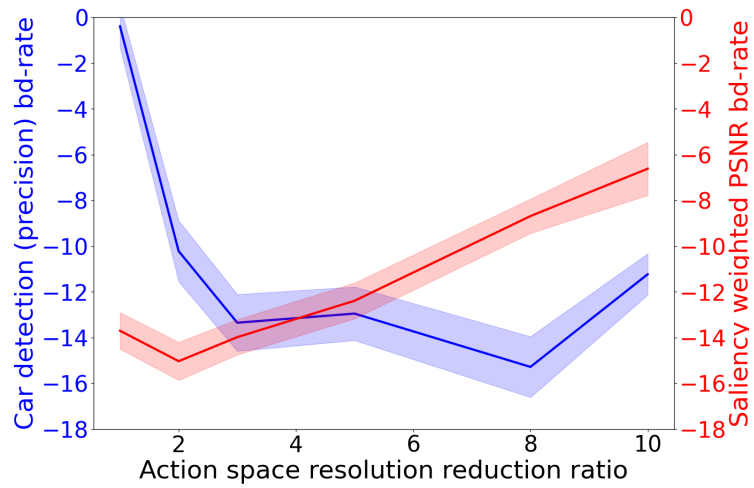


Figure 11: The effect of action space resolution on the BD-rate for both tasks

Train streams	
0000f77c-6257be58	000e0252-8523a4a9
000f157f-dab3a407	000f8d37-d4c09a0f
00a04f65-af2ab984	00a0f008-3c67908e
00a0f008-a315437f	00a1176f-0652080e
00a1176f-5121b501	00a2e3ca-5c856cde
00a2e3ca-62992459	00a2f5b6-d4217a96
00a395fe-d60c0b47	00a9cd6b-b39be004
00abd8a7-ecd6fc56	00abf44e-04004ca0
00adbb3f-7757d4ea	00afa5b2-c14a542f
00afa6b9-4efe0141	00b04b30-501822fa
00b1dfed-a89dbe2b	00be7020-457a6db4
00beeb02-ba0790aa	00c12bd0-bb46e479
00c29c52-f9524f1e	00c41a61-4ba25ad4
00c497ae-595d361b	00c87627-b7f6f46c
00ca8821-db8033d5	00cb28b9-08a22af7
00ccf2e8-59a6bfc9	00ccf2e8-ac055be6
00ccf2e8-f8c69860	00ce6f6d-50bbe62
00ce8219-12c6d905	00ce8219-d0b5582e
00cef86b-204ea619	00cef86b-d8d105b9
00cf8e3d-3d27efb0	00cf8e3d-4683d983
00cf8e3d-773de15e	00cf8e3d-a7b4978c
00d0f034-6d666f7b	00d18b13-52d3e4c4
00d4b6b7-7d0a60bf	00d4b6b7-a0b1a3e0
00d7268f-fd4487be	00d79c0a-23bea078
00d79c0a-a2b85ca4	00d84b1d-21e6fe01
00d8944b-e157478b	00d8d95a-74aa476a
00d9e313-7d75bb18	00d9e313-926b6698
00dc5030-237e7f71	00de601c-858a8a8d
00de601c-cfa2404b	00e49ed1-9d41220c
00e4cae5-c0582574	00e5e793-f94de032
00e81dcc-b1dd9e7b	00e8c106-e197c4b1
00c50078-6298b9c1	00b93c6e-6298aa25
0000f77c-cb820c98	

Table 9: List of streams used in training

Validation streams	
00d8d95a-47d98291	00e02d60-54df99d1
00a820ef-d655700e	00ce95b0-84be34a3
00d15d58-9197cde54	00b04b12-a7d7eb85
00c17a92-d4803287	

Table 10: List of streams used in validation

Test streams			
cd35ea13-f49ee278	cd389564-8be2128e	cdc05b0a-3bb83a9c	cd389564-9053f5fc
cd3b1173-63cb9e2e	cd3dab20-1b3e564e	cd3dab20-4ea3d971	cd3df92f-d04e142c
cd40cb21-18170d03	cd4ac25c-61a9eb11	cd4bf816-2abb75c9	cd4bf816-c2f9bf78
cd4ce4e5-6994fd2d	cd4ce4e5-d0968ec0	cd4da443-da4fe8c7	cd4deee2-0703d1c7
cd4deee2-1d9539bd	cd4deee2-37c8b95c	cd4deee2-3feadd6e	cd4deee2-60291439
cd4deee2-688c8bba	cd4deee2-8e12e5b5	cd4deee2-9c9f6da1	cd4deee2-adc7e92a
cd4deee2-ce4f69f5	cd4deee2-d078d54a	cd547736-3b63cb96	cd583365-462cca17
cd5a94cf-345f214a	cd5a9e1b-86faac85	cd5b2540-465c9328	cd5b2540-913cb8f7
cd5bee17-bef4f177	cd5db4e0-1189ff83	cd6af452-e54a1e36	cd6c087e-03ca2127
cd6fdd33-ac9cb2db	cd704168-1231930e	cd7c12c7-7029da5d	cd7c12c7-9b46c2a8
cd7e92a7-3b20257f	cd7c92a7-89b23268	cd7c92a7-9222ee19	cd7c92a7-ed0d3926
cd7ee0b1-dd286a1b	cd7fb8f1-3d347a66	cd828461-db8b4612	cd839842-cd859db0
cd8b00aa-4aac0701	cd8b00aa-5c017145	cd8b00aa-f00ad3b9	cd8b30b0-51369077
cd8b30b0-e8d12cc4	cd8d2fde-2d2a3211	cd9b6b86-9f62a970	cd9b6b86-be582832
cd9cd3dd-d67bf5b6	cd9d84d4-f59d3feb	cd9dff27-94731aba	cd9e7e2b-4b274850
cda33556-28510da1	cda33556-8dc294b4	cda33556-c6b3dd45	cda55704-362ddfea
cda55704-754aac99	cda63e8d-0afb52b	cda63e8d-76b2fa43	cda9acc1-1a92349d
cda9acc1-4469e473	cda9acc1-9d1ef61a	cdac4037-afed765d	cdac7315-fe37a1d9
cdae6e60-0fb06a75	cdae6e60-334ffc87	cdae6e60-b729f2e6	cdae377-1eccb13a
cdae377-2263611a	cdae377-2b38ae2c	cdb06fa9-cfb70e11	cdb06fa9-eba5643a
cdb3b01b-673f85b7	cdb616df-393f382c	cdb688d4-33f24ca3	cdb6b049-c96359c8
cdb815da-d03b9395	cdb992be-f0f1613c	cdbb20a9-bdab1f4e	cdbbac37-49c0a335
cdbc7842-b72c4915	cbd1882-bdd416ea	cdbeedfd-4ab64af8	cdfb4bd1-0c65ed7a
cdc05b0a-3bb83a9c	cdc05b0a-c53c36a6	cdc05b0a-c6e8b6ec	cdc05b0a-ce908cf7
cdc05b0a-d4ff800b	cd3dab20-1b3e564e	cdc05b0a-efb78be5	cdc05b0a-f2a67b44

Table 11: List of streams used in test